Robotica (2002) volume 20, pp. 529–535. © 2002 Cambridge University Press
DOI: 10.1017/S0263574702004289 Printed in the United Kingdom

Orientation capability representation and application to manipulator analysis and synthesis

Paresh Shah and Jian S. Dai*

Department of Mechanical Engineering, School of Physical Sciences and Engineering, King's College, University of London, London WC2R 2LS (United Kingdom). E-mail: Jian.Dai@kcl.ac.uk and Paresh.Shah@kcl.ac.uk

(Received in Final Form: March 16, 2002)

SUMMARY

This paper proposes a new orientation representation of planar manipulators by resorting to polar coordinates. Connecting the end-effector point to the first joint of a manipulator with a virtual adjustable link, the length of the adjustable link corresponds to a workspace point and is related to the orientation of the end effector link by a virtual angle in the form of a transcendental equation. Plotting this link length against the virtual angle in polar coordinates, the orientation of a manipulator can be represented in a compact form, and the range of partial dexterity can be identified. The characteristics of the new representation is hence revealed and related to the assessment of an orientation capability of a manipulator. Based on this representation, a desirable task can be presented and a manipulator can be synthesised with the required orientation.

KEYWORDS: Orientation; Dexterity; Representation; Analysis; Synthesis; Serial manipulator.

1. INTRODUCTION

There is a growing interest in manipulator synthesis based on the orientation capability with which an anticipated manipulator can carry out a desirable task with a certain orientation. In most cases, manipulator synthesis is based on a dexterous workspace about which a manipulator can rotate the end-effector a full turn while the end-effector point remains at the same point. Identification of a dexterous workspace[1] has been developed resulting in several geometric approaches. Davidson and Pingali[2] investigated the trajectory of a plane fixed at an end-effector to generate a dexterous workspace. They further used right-armed and left-armed closure[3] to depict a dexterous workspace. Dai *et al.*[4] developed an approach by projecting a higher-dimensional finite twist mapping onto a reachable workspace to obtain a dexterous workspace.

Hence the dexterous workspace can be presented as an enclosed area of a reachable workspace. The manipulator synthesis is then implemented in this area. Lu and Cai[5] introduced a dexterity chart to determine the robot hand kinematic parameters and to evaluate the grasping movement. Davidson and Chaney[6,7] synthesised a manipulator by fixing the mounting angle of a manipulator with determined radial location and orientation of a workspace. In a similar way to a manipulator synthesis, Soylu and Kanberoglu[8] designed a crank-rocker linkage based on the crank rotatability[9,10] region map which was generated from those conditions where only non-real roots were produced from the Freudenstein's equation.[11]

Manipulator synthesis based on a requirement of a certain orientation rests on the orientation capability representation in which a certain range of orientation can be achieved. The current representation is based on a composite representation[12] in which a reachable workspace point is related to the orientation of an end-effector at the point. A further representation is proposed by Dai *et al.*[4] based on the finite twist representation of an end-effector which has one dimension to depict an orientation of a planar manipulator. These representations are in a three-dimensional image space and have a difficulty in manipulator synthesis where planar manipulator operates in a two-dimensional physical space.

Integration[13,14] of orientation study to the rotatability study[15] raises the potential of generating a compact representation which is consistent[16] with the physical space a manipulator is operating and which is coherent on manipulator synthesis.

This paper proposes a new representation which gives the orientation capability of a planar manipulator in the form of polar map. In which, the Cartesian reachable workspace is integrated in the polar representation with the orientation angle of an end-effector. With the norm of a radius vector representing the length of a virtual adjustable link, the angle representing the angular displacement of the virtual joint rotation, the polar map relates the manipulator parameters to the orientation presentation with its two boundary loci. The paper gives the geometry of the map and presents manipulator synthesis with case studies. The study is based on boundless joint angles and the extension to bounded joint angles will be given elsewhere.

2. ORIENTATION ANGLE AND ITS PARAMETRIC REPRESENTATION

An orientation angle of a manipulator can be associated with a corresponding closed-loop mechanism. This is achieved by connecting the end-effector to the first joint of a manipulator with a virtual ground link. The virtual link l_v is adjustable and reflects the reachable workspace point. A virtual joint is located at the end-effector and a virtual angle, θ_v, is obtained. This gives the orientation of a manipulator.

* Corresponding author.

https://doi.org/10.1017/S0263574702004289 Published online by Cambridge University Press

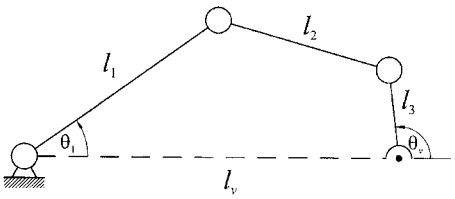


Fig. 1. Three-link manipulator with an imaginary adjustable ground link l_v.

Hence, the orientation can be related to manipulator parameters as

$$\cos\ \theta_v = f(l_1, l_2, l_3 \ldots l_n, l_v). \tag{1}$$

Figure 1 gives a planar three-link manipulator with an adjustable link to form a virtual four-bar mechanism. Implementing the vector closure loop based method,[17] similar to that derived by Williams II and Reinholtz[18] but taking θ_v as an input angle, an orientation equation for the virtual mechanism can be derived as

$$\cos\ \theta_v = \frac{1}{l_v}\left(\frac{l_1^2 + l_2^2 - l_3^2 \pm 2l_1l_2}{2l_3}\right) - l_v\frac{1}{2l_3}. \tag{2}$$

The equation can be used to identify the rotatability of the end-effector link with orientation angle θ_v and hence to decompose the reachable workspace into regions according to orientation capability. When the value of the equation falls within [–1, 1] range, the solution for the virtual angle is a real number. This limits the orientation ranges of the end-effectors. The area is categorised as having partial dexterity. When the value of the equation falls outside [–1, 1] range, the solutions for the virtual angle are complex numbers. The workspace area has full dexterity. The criterion can be extended to identify the workspace of manipulators with a higher number of links.

3. ORIENTATION POLAR MAP

Plotting Equation 2 in polar coordinates with distance r representing l_v and angle θ representing θ_v, the relationship of these two parameters leads to

$$\cos\ \theta = \frac{\mathrm{A}}{r} - r\mathrm{B}, \tag{3}$$

where $A = \dfrac{l_1^2 + l_2^2 - l_3^2 \pm 2l_1l_2}{2l_3}$ and $B = \dfrac{1}{2l_3}$.

For every r there exist two real number solutions, or two complex number solutions or mixed solutions. The two real number solutions give the orientation limits of the end-effector link. When the complex number solutions are obtained, the end-effector link can have a full turn at the point which is represented by the radius vector, r. The workspace point therefore has a full dexterity. When one complex number and one real number solution are obtained, the real number gives the orientation change point at which the manipulator does not have continuing orientation. The workspace is still classified as being partially dexterous. These give a set of orientation ranges with respect to changed values of l_v. More points can be produced with loci of l_v. By connecting these points, two offset concentric circles can be drawn as in Figure 2, where the two circles are offset against the origin along the Ox line.

In the map, the outermost and innermost circles which are centred at the origin represent the boundaries of the reachable workspace. The orientation boundary is made up of two offset concentric circles. This constitutes the orientation annulus represented by the lower boundary of r_{ol} and upper boundary of r_{ou}. The orientation annulus hence gives both partial and full dexterous workspace area.

An orientation polar map is hence produced with a two-dimensional composite representation of position and orientation in terms of the virtual adjustable link l_v and the virtual angle θ_v.

The polar equation of the locus which is given when an end-effector position is fixed is a circle centred at the origin. The intersection between the orientation annulus and the end-effector locus represents the orientation range for a manipulator at a certain reachable workspace range. The full dexterous workspace appears when the end-effector does not intersect the boundary of the orientation space. This gives a dexterous workspace annulus in Figure 3.

The area represented by this annulus has full dexterity, as there are no real number solutions for the virtual angle θ_v.

4. CHARACTERISTICS OF THE ORIENTATION POLAR MAP

In the orientation polar map, the orientation annulus is produced. The characteristics of this annulus can be obtained from the following analysis.

This starts from a three-link manipulator. Taking the end-effector positions which constitute loci a and b in Figure 4. The intersection between these loci and one locus of the orientation annulus can be given in the figure. The two intersections, $\mathrm{P_A}$ and $\mathrm{P_B}$, have different l_v values but the same orientation represented by the same orientation locus.

Giving the offset of the orientation annulus as s_0 and equating the norms of vector, t_a and t_b at the intersections, it follows.

$$s_0^2 + l_{va}^2 - 2s_0l_{va}\cos\ \theta_{va} = s_0^2 + l_{vb}^2 - 2s_0l_{vb}\cos\ \theta_{vb}. \tag{4}$$

Solving the above equation gives,

$$s_0 = \frac{l_{va}^2 - l_{vb}^2}{2l_{va}\cos\ \theta_{va} - 2l_{vb}\cos\ \theta_{vb}}. \tag{5}$$

Substituting Equation (2) with both orientation angles θ_{va} and θ_{vb} into the above yields

$$s_0 = \frac{l_{va}^2 - l_{vb}^2}{\left[\dfrac{l_1^2 + l_2^2 - l_3^2 \pm 2l_1l_2 - l_{va}^2 - l_1^2 - l_2^2 + l_3^2 \mp 2l_1l_2 + l_{vb}^2}{l_3}\right]} = -l_3. \tag{6}$$

https://doi.org/10.1017/S0263574702004289 Published online by Cambridge University Press

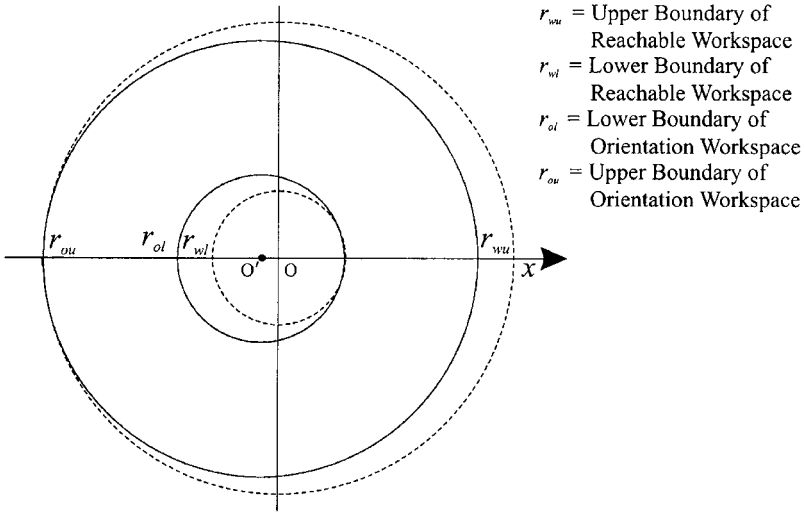


Fig. 2. An orientation map with a reachable workspace and an orientation annulus.

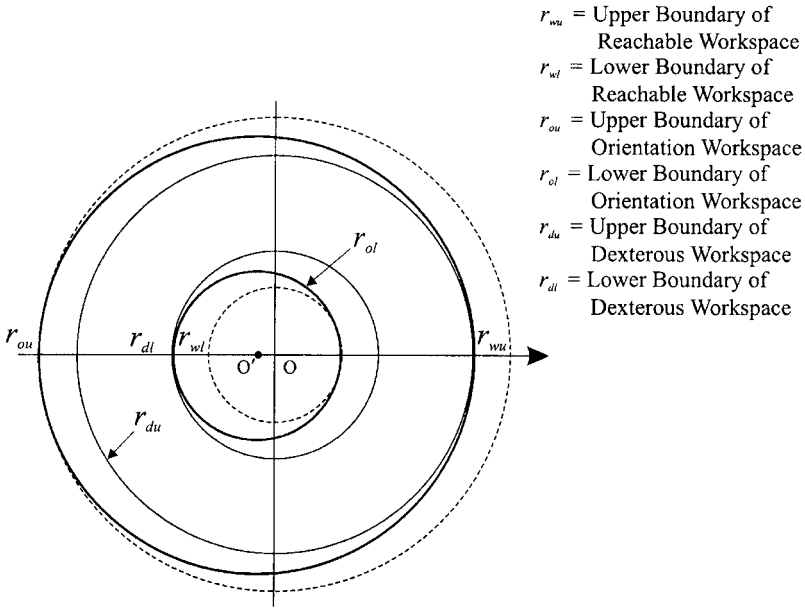


Fig. 3. Orientation and dexterous annulus in the orientation polar map.

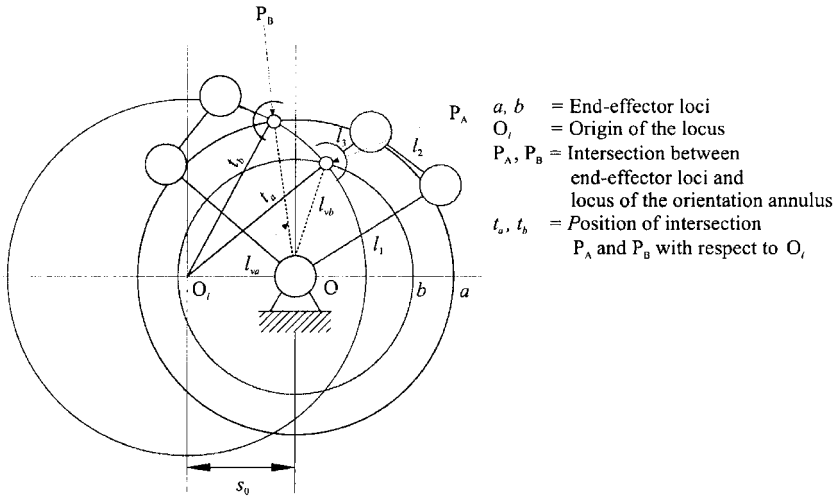


Fig. 4. Characteristics of the orientation polar map.

https://doi.org/10.1017/S0263574702004289 Published online by Cambridge University Press

This gives the offset value as the link length of the last link l_3. The radii of the boundary of the orientation annulus can hence be given by resolving triangle O′P_AO. This gives.

$$r^2=t_a^2=t_b^2=l_v^2+l_3^2+2l_vl_3\left(\frac{l_1^2+l_2^2-l_3^2\pm 2l_1l_2-l_v^2}{2l_3l_v}\right), \quad (7)$$

which on simplification yields,

$$r_{ou}=l_1+l_2, \quad (8)$$

$$r_{ol}=|l_1-l_2|. \quad (9)$$

Hence the radii of the two concentric circles centred at O′ are given as $|l_1-l_2|$ and l_1+l_2.

When a manipulator has more than three links, virtual proximate link l_{12} can be introduced. The above result can be applied by replacing link l_1 with the virtual proximate link and the offset value, s_0 can be generated again with respect to the length of the last link.

This can be demonstrated from the following. For the sake of argument, a four-link manipulator is given in Figure 5.

The virtual proximate link l_{12} is introduced and defined as $\sqrt{l_1^2+l_2^2-2l_1l_2\cos\beta}$. with the value of the virtual link varying between $|l_1-l_2|$ and l_1+l_2. Substituting the above-mentioned values into Equation 5, the following is given

$$s_o=\frac{l_{va}^2-l_{vb}^2}{2(p_1-p_2)}, \quad (10)$$

where

$$p_1=l_{vb}\left(\frac{(l_1^2+l_2^2-2l_1l_2\cos\beta)+l_3^2-l_4^2\pm 2l_3\sqrt{(l_1^2+l_2^2-2l_1l_2\cos\beta)}+l_{vb}^2}{2l_4l_{vb}}\right)$$

and

$$p_2=l_{va}\left(\frac{(l_1^2+l_2^2-2l_1l_2\cos\beta)+l_3^2-l_4^2\pm 2l_3\sqrt{(l_1^2+l_2^2-2l_1l_2\cos\beta)}+l_{va}^2}{2l_4l_{va}}\right).$$

This on simplification gives the value of s_o as $-l_4$.

Hence the offset value is defined by the length of the last link. The radii of the boundary of the orientation workspace can be characterised by substituting the above equation as follows

$$r^2=l_v^2+l_4^2+2l_vl_4$$

$$\times\left(\frac{l_1^2+l_2^2+2l_1l_2\cos\beta)+l_3^2-l_4^2\pm 2l_3\sqrt{(l_1^2+l_2^2+2l_1l_2\cos\beta)}-l_v^2}{2l_4l_v}\right). \quad (11)$$

Which on simplification yields,

$$r=\sqrt{(l_1^2+l_2^2+2l_1l_2\cos\beta)}\pm l_3. \quad (12)$$

Since $\cos\beta$ varies between -1 and 1, we have the following results,

$$r_{ou}=l_1+l_2+l_3, \quad (13)$$

$$r_{ol}=|l_1-l_2|-l_3\geq 0. \quad (14)$$

Hence the orientation annulus of a planar serial manipulator can be obtained directly from manipulator parameters and the orientation capability can be given in the polar map.

5. ORIENTATION ANALYSIS OF SERIAL MANIPULATORS

With a given manipulator, an orientation map is uniquely fixed as in Figure 2. The orientation capability can be obtained and the dexterous workspace can be presented. With a certain end-effector point, the orientation range can hence be identified from the map.

For the illustration purpose, two manipulators are given with different number of links. The first manipulator is a three-link manipulator with link lengths, $l_1=90$ mm, $l_2=40$ mm and $l_3=10$ mm. Hence the geometric parameters of the orientation map can be given as $s_0=-10$ mm, $r_{ol}=50$ mm and $r_{ou}=130$ mm from Equations 6, 8 and 9. This generates the orientation map in Figure 6.

In the figure, the manipulator workspace is defined by the norm of the virtual link. This can be represented as a distance in the figure and plotted as a locus of the end-effector in polar coordinates. The intersection of this locus with the boundary of the orientation annulus gives the orientation range with a specific end-effector position. This represents the virtual link length of 50 mm.

The intersection of this locus with the orientation boundary, r_{ol}, gives points A and B. Hence the orientation

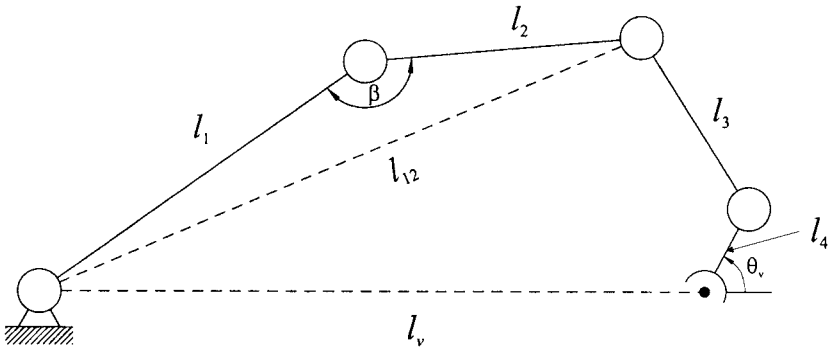


Fig. 5. Four-link manipulator with a virtual proximate link and a virtual adjustable ground link.

https://doi.org/10.1017/S0263574702004289 Published online by Cambridge University Press

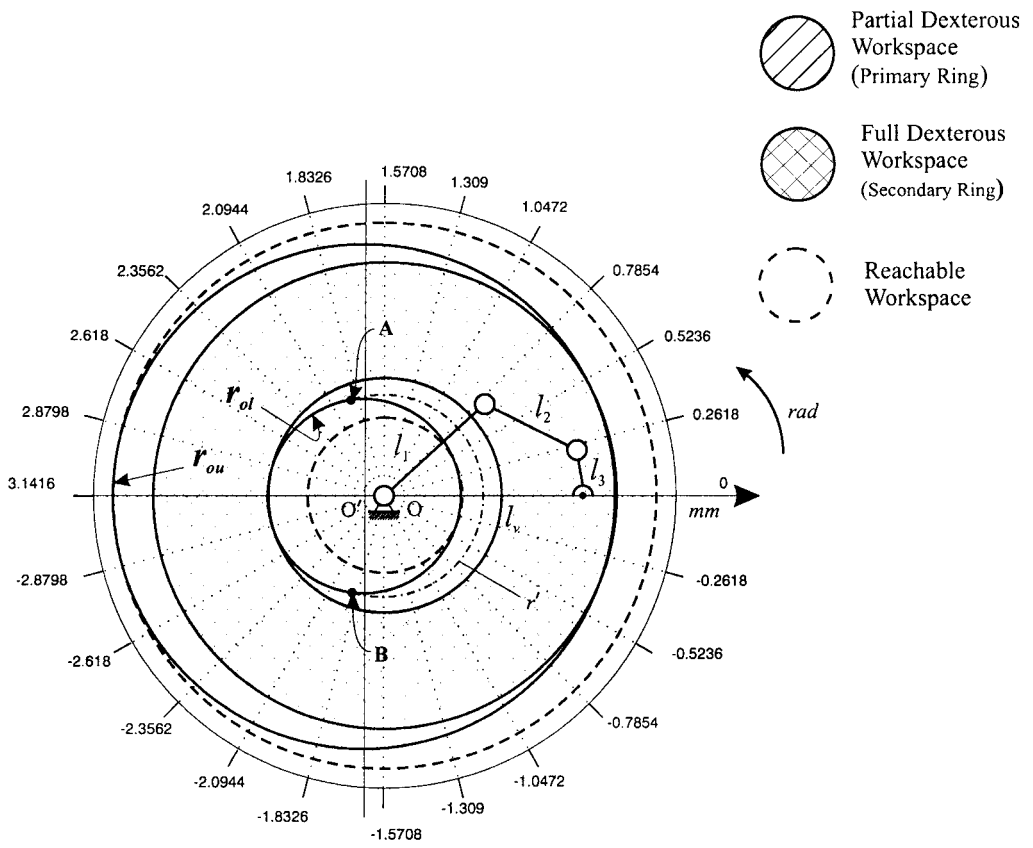


Fig. 6. Orientation map of a three-link manipulator.

range is -1.8 rad to 1.8 rad when the end-effector is at $r=50$ mm locus. The areas of orientation can be calculated from the enclosed crescent formed by arc(AB) and arc r'.

The second manipulator is a four-link manipulator with link lengths, $l_1=80$ mm, $l_2=70$ mm, $l_3=50$ mm, $l_4=30$ mm and $\delta=40$ mm, where δ is the radius of the vicinity limit circle around the first joint of a manipulator which is unacceptable due to the physical limitation. The geometric parameters of the orientation polar map can hence be obtained from Equations 10, 13 and 14 as $s_0=-30$ mm, $r_{ou}=200$ mm and $r_{ol}=0$ mm. This generates an orientation map in Figure 7.

The orientation annulus is defined by the loci, r_{ol} and r_{ou}. Since the vicinity limit δ, the lower boundary of the

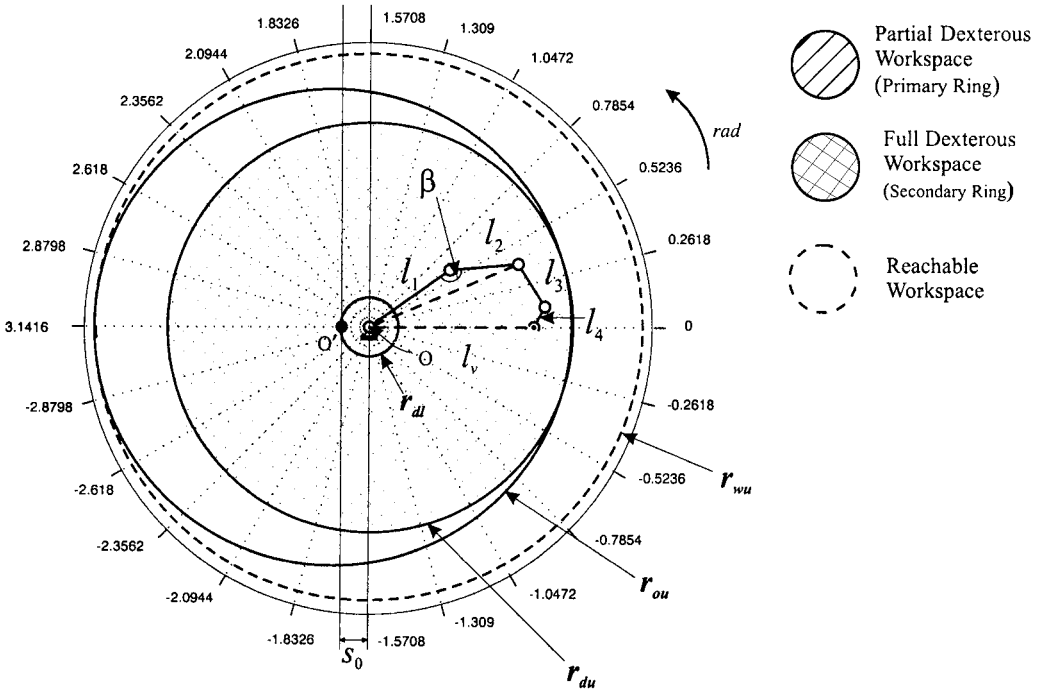


Fig. 7. Orientation map of a four-link manipulator.

https://doi.org/10.1017/S0263574702004289 Published online by Cambridge University Press

orientation annulus is r_{ou}. This results in a dexterous annulus r_{dl} and r_{du}.

6. ORIENTATION ORIENTED SYNTHESIS

The characteristics of the orientation polar map are directly related to manipulator parameters and can hence be used for manipulator synthesis. This synthesis is based on the orientation requirement of a given task. This starts by mapping the workspace into polar coordinates. With a given task with reachable workspace points and corresponding orientation requirements, the task can be mapped as polar equations of loci and the orientation range is mapped as vectorial angles. Hence a task crescent can be obtained as in Figure 8.

The width of the task crescent is equal to $b=r_{tu}-r_{tl}$, where r_{tu} is the upper limit of the task crescent and r_{tl} is the lower limit of the task crescent. With the given task crescent a desirable manipulator can be obtained. This starts by obtaining the orientation map of the manipulator. From two task points in polar coordinates (r_a, θ_a) and (r_b, θ_b), the offset of the orientation annulus can be given from Equation 5 as

$$s_0=\frac{r_a^2-r_b^2}{2(r_a\cos\theta_{va}-r_b\cos\theta_{vb})}. \tag{15}$$

From triangle O′AO in the figure, the lower boundary of the orientation annulus can be obtained as

$$r_{ol}=\sqrt{r_a^2+s_0^2+2r_as_0\cos\theta_a}. \tag{16}$$

The upper boundary of the orientation annulus can be obtained as

$$r_{ou}=s_0+r_{tl}+b. \tag{17}$$

Hence, from Equations 6, 8 and 9, manipulator parameters can be obtained. When a four-link manipulator is required, manipulator parameters can be obtained by Equations 10, 13 and 14.

The procedure can be summarized as

(i) define a task crescent in polar coordinates;
(ii) identify the parameters of the task crescent;

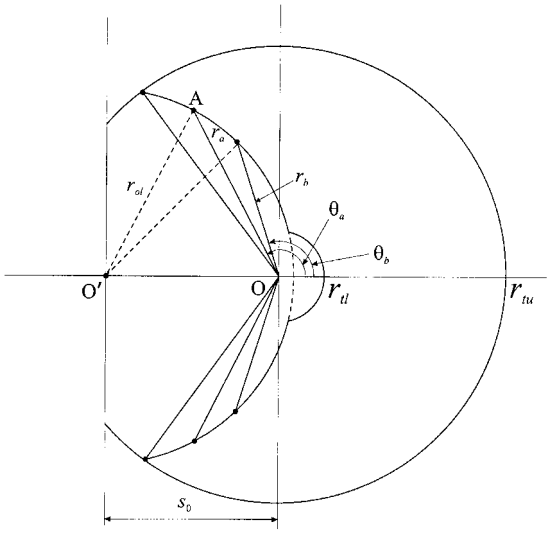


Fig. 8. Orientation map of a task.

(iii) determine the orientation annulus;
(iv) obtain manipulator parameters from the orientation annulus.

An example is illustrated with a required task which can be mapped in polar coordinates as a task crescent in Figure 8. The task is that of a partial dexterous workspace with the end-effector having an orientation range between 45° and 60° in the workspace. Representing the task in the polar map, the following task-map parameters can be obtained. The task crescent boundaries r_{tu} and r_{tl} are given as 110 mm and 50 mm and the width b is 60 mm. From the task crescent orientation map a desirable manipulator can be identified and subsequent manipulator parameters can be determined. With two set of data in the task crescent, the orientation annulus can be obtained from Equations 15 to 17 as $s_0=-272.8$ mm, $r_{ol}=277.5$ mm and $r_{ou}=382.8$ mm.

Assuming that the manipulator has three links, this categorises the manipulator into either of the groups from group III to VI.[14] This produces the following relations

- $l_2/l_1>l_3>l_1/l_2$
- $l_1/l_2>l_3+l_2/l_1$

Hence the manipulator parameters can be obtained from the orientation annulus as $l_1=330$ mm, $l_2=52.6$ mm and $l_3=272.8$ mm. The resultant manipulator with its orientation annulus and task crescent is given in Figure 9.

7. CONCLUSIONS

This paper has proposed a new way of examining the orientation capability of serial manipulators by introducing a virtual adjustable ground link that converts the orientation study of a serial manipulator into that of an equivalent mechanism. The parameters of the virtual link correspond to the reachable workspace point and the orientation angle of the end-effector link is related to the rotatability of the mechanism. Both virtual link length and orientation angle are related to manipulator parameters.

Having examined the rotatability of the equivalent mechanism, a new orientation map is developed relating the parameter of the virtual link to the orientation angle. The map is based in polar coordinates and relates the Cartesian space to the orientation capability. The characteristics of the map have been analysed with two orientation boundary loci which are horizontally offset from the origin and which are related to manipulator parameters. With the manipulator representation centred at the origin of the polar map, the orientation capability range can be identified by the intersection between the orientation boundary loci and the centre located circle represented by the trace of the virtual adjustable link. This creates the orientation capability of a manipulator at each part of the reachable workspace.

With this compact and coherent map, the manipulator synthesis with desirable orientation capability can hence be implemented. The task is mapped into polar coordinates as a task crescent with required orientation. This subsequently generates the orientation annulus of a desirable manipulator. From the orientation annulus the manipulator can be

https://doi.org/10.1017/S0263574702004289 Published online by Cambridge University Press

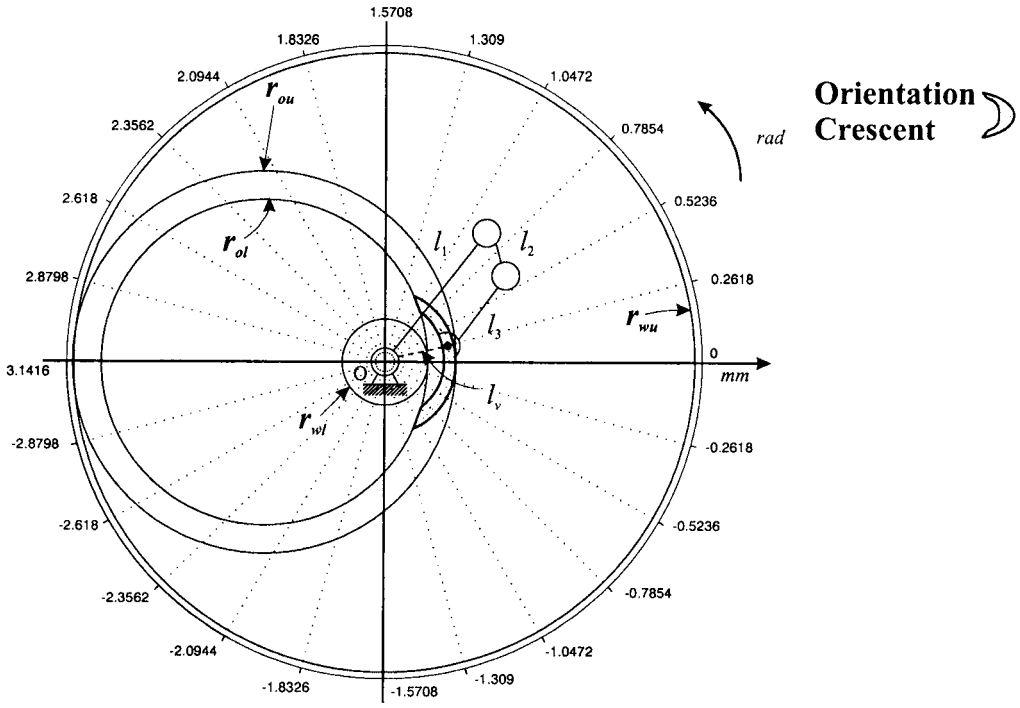


Fig. 9. Resultant manipulator and its orientation polar map from a task crescent.

obtained. Examples were used to illustrate the orientation analysis and the synthesis procedure.

ACKNOWLEDGEMENT

The financial support from the Engineering and Physical Science Research Council (EPSRC) under grant number GR/R26443 is gratefully acknowledged.

References

1. A. Kumar and K. Waldron, "The Dexterous Workspace", *ASME paper No. 80-DET* (1980).
2. J. Davidson and P. Pinga, "Robot workspace of a tool plane Part II: computer generation and selected design conditions for dexterity", *ASME Journal of Mechanism, Transmissions and Automations in Design* **109**, 61–71 (1987).
3. J. K. Davidson, "A Synthesis Procedure for Design of 3-R Planar Robotic Workcells in which Large Rotations are required at the Workpiece", *ASMF Journal of Mechanical Design* **114**, 547–558 (1992).
4. J. Dai, N. Holland, and D. Kerr, "Finite Twist mapping and its application to planar serial manipulators with revolute joints", *Journal of Mechanical Engineering Science, Proceedings of Institution of Mechanical Engineers, Part C* **209**, 263–271 (1995).
5. L. Lu and C. Cai, "Object oriented dexterity analysis and design application for planar robot hands", *20th ASME Biennial Mechanisms Conference* **15**, 155–162 (1988).
6. J. K. Davidson and K. D. Chaney, "A synthesis method for placing workpieces in RPR planar robotic workcells", *ASME Journal of Mechanical Design* **120**, 262–268 (1998).
7. J. K. Davidson and K. D. Chaney, "A design procedure for RPR planar robotic workcells: an algebraic approach", *Mechanism and Machine Theory* **34**, 193–203 (1999).
8. R. Soylu and K. Kanberoglu, "Analysis synthesis of mechanisms – Part 2: Crank-rotatibility synthesis", *Mechanism and Machine Theory* **28**, 835–844 (1991).
9. J. H. Shyu and K. Ting, "Invariant Link Rotatbility of N-Bar Kinematic Chains", *ASME Journal of Mechanism, Transmissions and Automation in Design* **116**, 343–346 (1994).
10. K. Ting, "Five-Bar Grashof Criteria", *ASME Journal of Mechanism, Transmissions and Automation in Design* **108**, 533–537 (1986).
11. Q. L. Woo and F. Freudenstein, "Application of Line Geometry to Theoritical Kinematic and the Mechanical System", *Journal of Mechanism* **5**, 417–460 (1965).
12. F.-C. Yang and E. Haug, "Numerical Analysis of the Kinematic Working Capability of Mechanisms", *Journal of Mechanical Design* **116**, 111–118 (1994).
13. N. A. Soman and J. Davidson, "A Two-Dimensional Formulation for Path-Placement in the Workcell of Planar 3-R robots", *ASME Journal of Mechanical Design* **117**, 479–484 (1995).
14. J. S. Dai and P. Shah, "Orientation Capability of Planar Serial Manipulators Using Rotatability Analysis Based On Workspace Decomposition" *Proc. IMechE, Part C, Journal of Mechanical Engineering Science* **216**(C3), 275–288 (2002).
15. D. Kohli and A. Khonji, "Grashof-Type Rotatability Criteria of Spherical Five-Bar Linkages", *Journal of Mechanical Design* **116**, 99–104 (1994).
16. J. S. Dai and J. Rees Jones, "Null space construction using cofactors from a screw algebra context" (*To appear in the Proceedings of the Royal Society: Mathematical, Physical and Engineering Sciences*, 2002).
17. H. Mabie and C. Reinholtz, *Mechanisms and Dynamics of Machinery* (Wiley, New York, 4th edition, 1986).
18. R. Williams II and C. Reinholtz, "Proof of Grashof's Law Using Polynomial Discriminants", *ASME Journal of Mechanisms, Transmissions, and Automation in Design* **108**, 562–564 (1986).

https://doi.org/10.1017/S0263574702004289 Published online by Cambridge University Press